Nuclear Instruments and Methods in Physics Research B 407 (2017) 297–303

Contents lists available at ScienceDirect

Nuclear Instruments and Methods in Physics Research B

journal homepage: www.elsevier.com/locate/nimb

Reaction measurements with the Jet Experiments in Nuclear Structure and Astrophysics (JENSA) gas jet target ☆

K.A. Chipps

Physics Division, Oak Ridge National Laboratory, Oak Ridge, TN 37831, USA
JENSA Collaboration

ARTICLE INFO

Article history:
Received 3 July 2017
Received in revised form 21 July 2017
Accepted 24 July 2017

Peer-review under responsibility of the Scientific Committee of the Conference on the Application of Accelerators in Research and Industry.

Keywords:
Astrophysics
Indirect measurements
Transfer reactions
Gas jet target

ABSTRACT

Explosive stellar environments are sometimes driven by nuclear reactions on short-lived, radioactive nuclei. These reactions often drive the stellar explosion, alter the observable light curves produced, and dictate the final abundances of the isotopes created. Unfortunately, many reaction rates at stellar temperatures cannot be directly measured in the laboratory, due to the physical limitations of ultra-low cross sections and high background rates. An additional complication arises because many of the important reactions involve radioactive nuclei which have lifetimes too short to be made into a target. As such, direct reactions require very intense and pure beams of exotic nuclei. Indirect approaches with both stable and radioactive beams can, however, provide crucial information on the nuclei involved in these astrophysical reactions.

A major development toward both direct and indirect studies of nuclear reactions rates is the commissioning of the Jet Experiments in Nuclear Structure and Astrophysics (JENSA) supersonic gas jet target. The JENSA system provides a pure, homogeneous, highly localized, dense, and robust gaseous target for radioactive ion beam studies. Charged-particle reactions measurements made with gas jet targets can be cleaner and display better resolution than with traditional targets. With the availability of pure and localized gas jet targets in combination with developments in exotic radioactive ion beams and next-generation detector systems, the range of reaction studies that are experimentally possible is vastly expanded. Various representative cases will be discussed.

1. Introduction

1.1. Explosive astrophysical scenarios

Many different explosive astrophysical environments exist and are thought to contribute to the elements observed today. Supernova explosions, the most energetic and likely the most widely recognized of these environments, occur when a massive star runs out of the hydrogen and helium it needs to sustain itself, resulting in collapse. This rapid collapse under the star's own gravitational pull ends abruptly when electron degeneracy pressure is reached, the result being a "bounce" and an immense shockwave of superheated material sent outward at thousands of kilometers per second. High neutron and neutrino fluxes are experienced as well, driving multitudes of nuclear reactions in the stellar ashes and ultimately dispersing them into the interstellar medium. Other supernova mechanisms involve accretion from a neighboring star. In each of these cases, intense neutron fluxes combined with the seed nuclei from sequential alpha captures in the earlier, helium-rich stellar environment push the creation of neutron-rich nuclei far past the valley of stability.

Novae, which peak around 0.3–0.4 GK and are the next most energetic astrophysical explosions, are driven by thermonuclear runaway on a white dwarf star due to accreting material from a binary companion. Less energetic still are X-ray bursts - thermonuclear runaway on the surface of a neutron star in accreted material from a binary companion - which can reach peak temperatures of ~1 GK and repeatedly explode. These accretion-driven explosive scenarios involve a complex network of proton- and alpha-induced nuclear reactions on proton-rich nuclei up to, and perhaps even past, mass 40 in novae and mass 100 in X-ray bursts. Quiescent burning in massive stars can also produce a variety of relative isotopic abundances seeded into the interstellar medium. In addition to these known sources of radioactive isotopes in the universe, even stranger scenarios are becoming accessible to observational probing: Thorne-Zitkow objects, proposed to be a neutron star core

☆ Conference on the Application of Accelerators in Research and Industry, CAARI 2016, 30 October – 4 November 2016, Ft. Worth, TX, USA.

E-mail address: chippska@ornl.gov

http://dx.doi.org/10.1016/j.nimb.2017.07.023
0168-583X/

driving quiescent rapid-proton capture process (rp-process) burning while hidden inside the envelope of a red giant star, or the exotic environments of black hole mergers resulting in gravitational waves recently observed by the Laser Interferometer Gravitational-Wave Observatory (LIGO), as candidates sites for the r-process.

The combination of recent improvements in the observation of the radioisotope sky, and more detailed and reliable simulations of explosive astrophysical scenarios enabled by supercomputing, is pushing forward our understanding of the creation and evolution of the elements. Due to this progress, we also need to thoroughly examine and accurately quantify the nuclear physics important to this complete picture of the universe. Advances in nuclear astrophysics are being driven by several factors. One is high-resolution observations of the distinct gamma- ray signatures of astrophysically-produced radioisotopes like ^{26}Al [16–18,22,21] (a signature of ongoing nucleosynthesis in the Milky Way) and ^{56}Ni [12] a radioisotope produced in supernovae useful for diagnosing the explosion mechanism). Another is large libraries of X-ray burst light curves such as MINBAR [25] which allow for detailed study of differences in energy output. Observations of elemental abundances of individual metal-poor stars [13] which tell us about elemental abundances prior to seeding from supernova ashes also contribute to this progress. Also, careful measurements of the various isotopic ratios of presolar grains contained within meteorites [22,34,14,1], which are useful thermometers and chronometers of the nucleosynthesis in various stellar atmospheres, contribute greatly to the nuclear astrophysics field. Add to this the new computational models, which now contain magnetohydrodynamics, neutrino transport, nuclear reaction networks, and other relevant physics, and we are able to test the limits of the uncertainties within each individual model input.

While it is known that the heavy elements we see today were created in exploding stars [7], many of the exact mechanisms are still open questions. As one example, it is still unknown how much each of several astrophysical production sites, such as the massive Asymptotic Giant Branch (AGB) stars and novae, contributes to the ^{26}Al observed by space-based telescopes [27,5], despite years of study. Open questions like these are driving the field of nuclear astrophysics.

Because the astrophysical sites involved in the production of these isotopes are extreme in temperature, pressure, neutron flux, etc, many of the nuclear reactions taking place involve short-lived radioactive nuclei. Most of these nuclei decay too quickly to be made into a traditional target for nuclear physics studies. Instead, turning the reaction around to "inverse kinematics" and using a stable target of (generally) hydrogen or helium and a beam of the radioactive species, provides a means for continued reaction studies. Dedicated radioactive ion beam facilities, like FRIB, will ultimately produce the exotic beams needed to better understand astrophysical processes.

1.2. Reaction studies

Some of the nuclear reactions, on both stable or unstable nuclei, which power stellar explosions may be studied directly in the laboratory. These "direct reactions" often involve long measurement times to collect sufficient statistics to directly calculate the reaction cross section and from that the reaction rate. When such direct measurements can no longer be undertaken, for example because beam intensities or target densities are not high enough for sufficient counting statistics, indirect measurements are a useful tool to elucidate the specific properties of nuclear levels which could play a role in the astrophysical cross section. These indirect techniques work through the determination of masses, excitation and resonance energies, spins, angular momentum transfer, branching ratios, and spectroscopic information of the nuclei involved in the astrophysical reaction, which are then used to calculate the reaction rate [31,23,20,26,2,8,15,33]. Such indirect techniques include elastic and inelastic scattering, gamma spectroscopy, surrogate and Trojan Horse methods, accelerator mass spectrometry, mass measurements, decay spectroscopy, and particle transfer.

However, though indirect techniques provide a substantial benefit to the study of astrophysical nuclear reactions, they too suffer from certain difficulties inherent in the technique. One of the main issues arises from the use of a traditional target material for an in-beam study. Traditional targets, such as pure metallic foils, polymerized plastic films, implanted targets, and small gas "cells," can introduce unwanted reaction backgrounds and worsen measured energy resolution. These targets may absorb contaminants onto their surfaces, such as water vapor or vacuum pump oil; they may contain stoichiometric components necessary for target chemistry but troublesome for nuclear physics measurements (such as the carbon inherent in the polymerized plastics used as hydrogen targets); they may be brittle or sensitive to beam-induced damage and depletion; and they may require the use of backing materials or windows. In order to improve upon the state of reaction measurements for nuclear astrophysics, new target development was required, in particular for cases where light ion (hydrogen or helium) reactions were necessary. The intent of this paper is to discuss development of such a target, that involves the use of a jet of gas as the target and both normal and inverse kinematics to study some of the reactions of interest with low cross sections.

2. Gas jets

2.1. Operational principle

The basic idea of using a jet of gas as a target for ion beam studies originated in Germany several decades ago [6,30,4,19]. The principle of such a system design would be to provide a dense and localized gas target without the need for any containment materials (whether chemical or physical) which would degrade the energy and angle resolution of the beam and reaction products. By supplying a high pressure gas reservoir to a nozzle inside of a vacuum target chamber, a highly localized and dense stream of gas is produced. The gas expands very little as it exits the nozzle and flows through the vacuum [28,24], eventually being directed into a receiver backed by high-throughput compressors or pumps. Early results of reaction studies demonstrated the success of the technique, with particle spectra displaying improved energy resolution and lowered backgrounds [6,30,4,19] when compared with traditional transfer-reaction targets, even at 90° in the laboratory frame where previously detectors would be shadowed by the structure holding a traditional target.

2.2. Development

With radioactive ion beams for inverse kinematics, a new gas jet target was required, which could utilize a light-ion gas such as hydrogen or helium, and which could achieve a much higher gas density than was previously possible. The new Jet Experiments in Nuclear Structure and Astrophysics (JENSA) gas jet target was designed, built, and commissioned for this purpose. The JENSA target has achieved a world record density for a helium jet for ion beam studies [9]. Commissioning data from JENSA[9,10,3], some of which is shown in the next Section, demonstrate clearly the benefit of using a dense, pure, and localized gas target over traditional target technologies. For example, consider a hydrogen gas jet target and a solid, hydrogen-rich, plastic film C_2H_4 (in nuclear physics

parlance, CH_2) target: calculations using the semi-empirical stopping power code SRIM [29] show that 4 MeV alpha particles experience over an order of magnitude higher stopping power in C_2H_4 than in an equivalent areal density of H_2 gas. This higher stopping power translates into a worsened resolution for the detected reaction products, as it broadens the energy spread of both the incoming beam and the outgoing recoils.

3. The JENSA system

A detailed description of the Jet Experiments in Nuclear Structure and Astrophysics (JENSA) gas jet target system is given in Chipps et al. [9]; the reader is directed to that document for reference. Some upgrades have been made, however, since the system was moved from its commissioning location at Oak Ridge National Laboratory (ORNL) to its final home in the Reaccelerated 3 MeV (ReA3) experimental hall at the National Superconducting Cyclotron Laboratory (NSCL) on the campus of Michigan State University (MSU). The NSCL facility will soon transition to the world-class Facility for Rare Isotope Beams (FRIB).

Due to the difference in beam optics between the ORNL tandem-based Holifield Radioactive Ion Beam Facility (HRIBF) and the linac-based ReA3 facility, the pumping cube apertures were widened at all locations along the JENSA system. To account for the changes in the pressure profile caused by this increase in aperture diameter, a "re-entrant" aperture at the D1 location [9] was designed and installed. This aperture, shown in Fig. 1, is considerably longer than the original D1 aperture, effectively decreasing its conductance and increasing the pressure drop between the target chamber and the first downstream differential pumping cube.

A larger change in the JENSA system was the upgrade of the final pumping stage before the compressor inlet [9]. The four Ebara 40×20 multistage roots blowers were replaced with a system comprised of two Leybold DV650S screw pumps backed by a third Leybold DV650S screw pump, controlled with a custom-designed interlock panel. These pumps have the benefit of being "dry," in other words, the motor and shaft are hermetically sealed from the compression volume, such that the JENSA target gas never comes into contact with pump oil. This slightly increased the total volume of the JENSA system, but provided a much cleaner environment for the target gas.

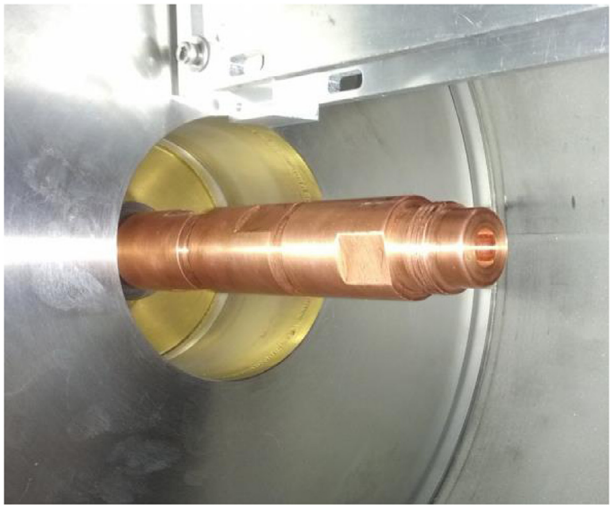

Fig. 1. Photograph of the new re-entrant aperture in the D1 (first downstream) location of JENSA. The aperture (copper) extends into the target chamber to decrease the aperture's conductance. Visible above the aperture is the mounting arm for the jet nozzle. Photo courtesy Justin Browne, MSU.

In order to fully utilize the JENSA gas jet target, a configurable mounting scheme for multiple types of charged- particle detectors was designed and fabricated, as seen in Fig. 2. In addition, a new linear drive was installed on the beam-right side of JENSA, which inserts either a 2×4 mm slit, a 4×4 mm slit, or a beam viewer (phosphor) into the gap between the jet nozzle and the receivers.

3.1. Recommissioning

Once the JENSA system was fully reinstalled on a dedicated beamline in the ReA3 hall (one of three beamlines), the system was recommissioned to confirm that the jet properties had not changed. Fig. 3 shows jet energy loss profiles (left panel) and the resulting densities (right panel) for the updated system. Shown are densities for several jet nozzle sizes, ranging in neck diameter between the two extremes originally described in Chipps et al. [9].

The recommissioning data from the ReA3/NSCL confirm the jet densities achieved during commissioning at ORNL [9].

3.2. Simulation packages

In order to facilitate the use of the JENSA gas jet target as a tool for reaction studies, a new version of the monte- carlo simulation code VIKAR [32], v4.0, was created. VIKAR 4.0 includes the option to simulate a reaction study with either a traditional foil target or a cylindrical gas jet target. The code accounts for the full reaction geometry, accurately simulating the non-flat energy loss profile that both the beam and reaction products encounter when interacting with a cylindrical jet. A standard JENSA setup file defining the geometry and operational parameters of the detector array is included with the code distribution.

4. Reaction measurements with JENSA

Several reaction measurements have been undertaken to date with JENSA, both at ORNL and at ReA3. These include:

^{120}Sn(^{14}N,^{14}N)^{120}Sn elastic scattering on a nitrogen jet[9], for commissioning purposes, to examine beam-jet overlap and operational parameters;
^{15}N(α,α)^{15}N elastic scattering on a helium jet, to help inform R-matrix calculations of the ^{15}N(α,p)^{18}O and ^{15}N(α,γ)^{19}F reaction cross sections;
the ^{14}N(α,p)^{17}O reaction on a helium jet, for commissioning purposes, to reproduce known cross sections for verification of target density data;
the ^{14}N(p,t)^{12}N transfer reaction on a nitrogen jet[10], to study the nuclear structure of particle- unbound levels in ^{12}N;
the ^{20}Ne(p,d)^{19}Ne transfer reaction on a neon jet [3], to determine information relevant to the ^{18}F(p,α)^{15}O astrophysical reaction rate;
the ^{20}Ne(p,t)^{18}Ne transfer reaction on a neon jet, to inform the ^{14}O(α,p)^{17}F astrophysical reaction rate;
and the first radioactive ion beam experiment with a gas jet target, an examination of the ^{34}Ar(α,p)^{37}K cross section relevant to X-ray bursts [11].

A selection of these reaction studies are described in more detail below.

4.1. ^{120}Sn+^{14}N elastic scattering

One of the early demonstrations of the JENSA system was a measurement of elastic scattering of 40 MeV ^{120}Sn on a natural nitrogen jet target (>99% ^{14}N), as described in Chipps et al. [9].

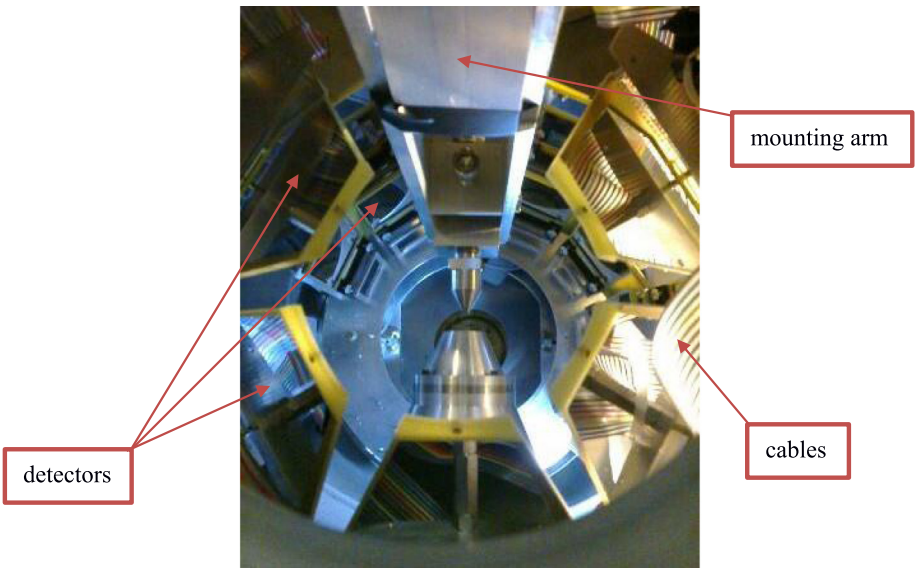

Fig. 2. View upstream of the new mounting hardware for segmented silicon detector arrays inside of the JENSA target chamber at ReA3.The detectors form several "rings" or "barrels" around the jet location. Also visible are some of the signal ribbon cables, the nozzle mounting arm (top), and the jet nozzle and receivers in the center of the image.

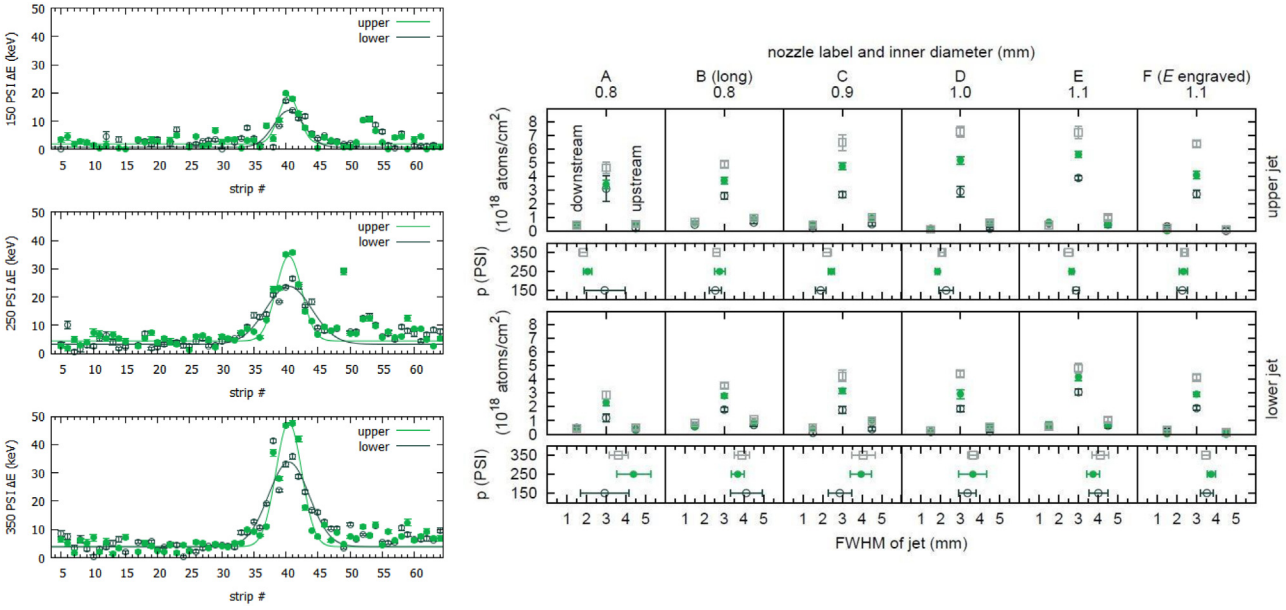

Fig. 3. Example jet energy loss profiles (left) for a 241Am alpha source and three different jet pressures of 150, 250, and 350 psig. The strip number corresponds to the position along the face of a highly-segmented silicon strip detector; see [9] for more details. The energy loss profile as measured on the detector is effectively a "projection" of the jet density. In each panel, corresponding to the different jet inlet pressures, density profiles from the top 4 mm of the jet ("upper," green) and bottom 4 mm of the jet ("lower," black) are shown. The lines are a best fit to the data. Right: density and size data for helium jets produced by six jet nozzles (labeled A-F) at the same three jet pressures. For each jet pressure (150psig, open black circles; 250psig, closed green circles; 350psig, open grey squares), the energy loss profiles are converted to areal density values through known stopping powers of alpha particles in the helium gas; the full width half maximum (FWHM) of the jet is determined from the known relation between the jet-detector distance and projection size. Uncertainties on the densities include statistical uncertainties and any uncertainties in the stopping power; uncertainties in the jet size (FWHM) account for the detector strip pitch (1.2 mm) and any uncertainties in the conversion from projection size to actual jet size. Densities measured just up- and downstream of the jet are shown as well. Images courtesy of Konrad Schmidt, MSU/NSCL. (For interpretation of the references to colour in this figure legend, the reader is referred to the web version of this article.)

The low-energy, heavy-mass beam was chosen to maximize the energy loss through the jet. Elastically-scattered particles can be seen past 80° in the laboratory frame, in contrast with traditional target foils where a large range around 90° is shadowed by a target frame and mounting structure, as well as reactions of interest disappearing (around 72°) behind the unwanted carbon component of the target material. Fig. 4 helps to elucidate this difference, though the reaction in each case is slightly different.

4.2. $^{14}N(p,t)^{12}N$

A benefit to using a gas jet target such as JENSA is the favorable ratio of target density to target-induced energy loss and straggling. Gas jets, thanks in large part to chemical purity, have very low stopping powers compared with traditional solid targets. This can allow for improved resolution over measurements utilizing traditional target materials.

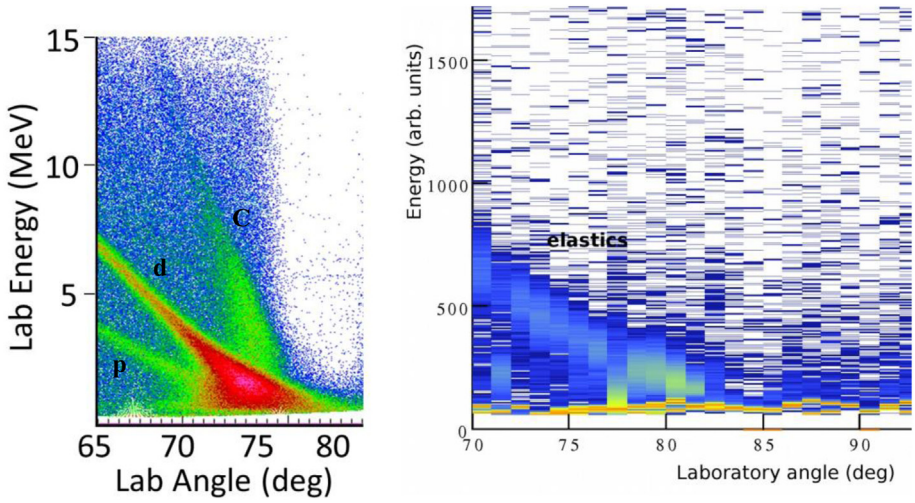

Fig. 4. Left: a typical elastic scattering spectrum from a deuterated plastic film target, showing kinematic lines from protons, deuterons, and carbon in the CD_2, and displaying the shadowing of the target ladder (the large white area on the right of the image). This target was used in a previous experiment to measure the (d,p) reaction on tin isotopes. Right: a $^{120}Sn+^{14}N$ elastic scattering spectrum from the JENSA jet, showing a single kinematic line from only the reaction of interest and no target ladder shadowing. The energy scale is ~3 keV per channel. Unlike in the left image, elastics are observable down to the electronics threshold. Similar behavior would be expected for a pure deuterium jet, which was unavailable at the time for a direct comparison. Left image courtesy of Steven D. Pain, ORNL; right panel adapted from Chipps et al. [9].

Shown in Fig. 5 is a zoomed-in triton energy spectrum from one SIDAR detector strip, focusing on the ground (furthest left), first excited (960 keV), and second excited (1191 keV) levels in ^{12}N (cf. [10]). The two excited states, though only about 200 keV apart, are completely separated in the charged particle spectra. The total experimental resolution is below 1%.

4.3. $^{20}Ne(p,d)^{19}Ne$

Another example transfer reaction with JENSA involved the successful determination of the spin and parity of a level in ^{19}Ne important for the $^{18}F(p,\alpha)^{15}O$ astrophysical reaction rate [3], possible thanks to jet purity [26]. An example spectrum is shown in Fig. 6.

Because the $^{18}F(p,\alpha)^{15}O$ reaction is difficult to measure directly, indirect methods, such as using particle transfer to populate the states of interest in the compound ^{19}Ne nucleus, must be used. Thanks to the purity of a neon gas jet target versus earlier attempts with an implanted target [26], the only contaminants in the particle spectra are from reactions on ^{22}Ne, which is a small natural component of neon gas. Enriched target gases would further improve such studies.

4.4. $^{34}Ar(\alpha,p)^{37}K$

The first radioactive ion beam experiment to use the JENSA gas jet target, or in fact any gas jet target, was undertaken in May of 2016 (cf. the proposal, Chipps et al. [11], for more details). A beam of ^{34}Ar was produced via fragmentation in the NSCL facility, stopped, and then reaccelerated to ~1.7 MeV/u in the ReA3 hall. Over 1100 channels of electronics, including charged particle detectors, gamma ray detectors, and beam normalization detectors were used in the measurement; a hybrid analog-digital data acquisition system was adopted.

As with the stable $^{120}Sn+^{14}N$ scattering measurement, in this case elastic scattering of $^{34}Ar+^{4}He$ was visible almost down to

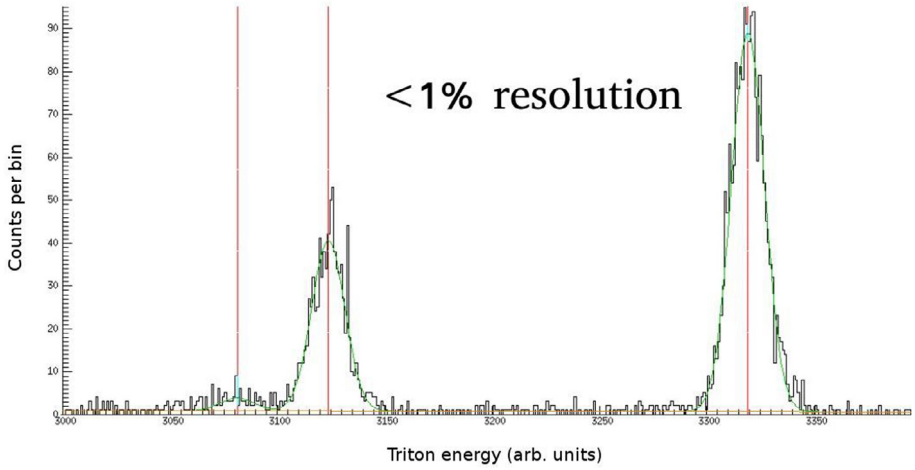

Fig. 5. Zoomed-in triton energy spectrum from the $^{14}N(p,t)^{12}N$ measurement of Chipps et al. [10], showing the low background and good energy resolution of the measurement. Data are shown in black; in green are Gaussian fits to the data, with the red lines marking the extracted centroids. The ground state peak at this angle falls at a triton energy of 14.6 MeV (right-most peak), and the first excited state at 13.7 MeV. Every level above the ground state is particle unbound. (For interpretation of the references to colour in this figure legend, the reader is referred to the web version of this article.)

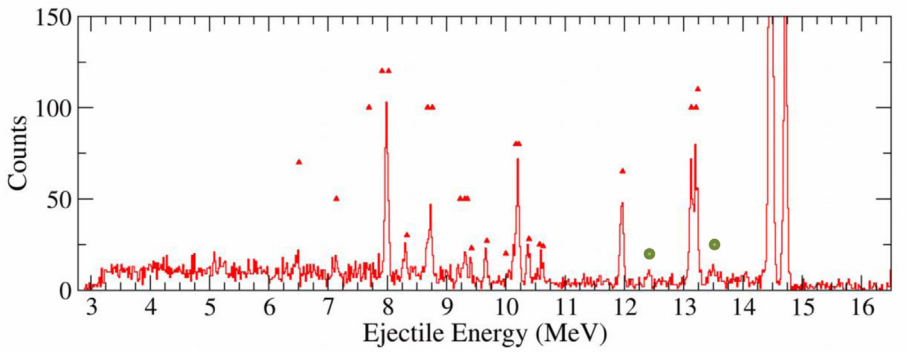

Fig. 6. Example deuterium energy spectrum from the ^{20}Ne(p,d)^{19}Ne reaction (red triangles mark expected levels) on a natural neon jet in JENSA [3]. The only contaminant peaks to be observed (green dots) are those from the ^{22}Ne(p,d)^{21}Ne reaction, as ^{22}Ne is about 9% of natural neon abundance. Figure courtesy of Daniel Bardayan. (For interpretation of the references to colour in this figure legend, the reader is referred to the web version of this article.)

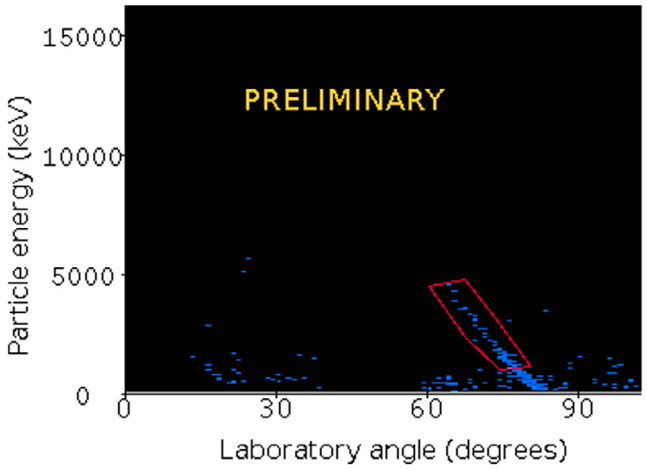

Fig. 7. Preliminary (online) data from the ^{34}Ar(α,p)^{37}K reaction measurement using JENSA and a radioactive beam from ReA3. Elastically-scattered alpha particles from the helium jet can be seen down to nearly 90° in the laboratory frame, thanks to the lack of shadowing from a traditional target and target frame.

90° in the laboratory, limited only by the electronics thresholds. This is demonstrated by the online data shown in Fig. 7. Extraction of the protons from the ^{34}Ar(α,p)^{37}K reaction of interest is ongoing.

5. Conclusion

As these cases for reactions using the Jet Experiments in Nuclear Structure and Astrophysics (JENSA) system demonstrate, there are many benefits to using a gas jet target for nuclear reaction measurements. Gas jet targets are dense, localized, pure, and robust; reaction measurements therefore benefit from improved energy and angular resolution, lowered target-induced backgrounds, and long-term target stability. Future measurements, as well as future improvements to JENSA, are planned; collaborations to build gas jet targets at other facilities worldwide have been formed.

Acknowledgements

The author would like to thank the staff at both the HRIBF and the NSCL/ReA3 facilities for their assistance in providing the beams used for this work, as well as the members of the JENSA Collaboration (jensajet.org) for their assistance in the operation of the experimental system and contributions to the work presented herein, in particular S. Ahn, D.W. Bardayan, J.C. Blackmon, J. Browne, U. Greife, F. Montes, P.D. O'Malley, W.J. Ong, S.D. Pain, W.A. Peters, H. Schatz, K. Schmidt, M.S. Smith, and P. Thompson. Research sponsored by the Laboratory Directed Research and Development Program of Oak Ridge National Laboratory, managed by UT-Battelle, LLC, for the U.S. Department of Energy under contract number DE-AC05-00OR22725. The work reviewed herein was supported by U.S. Department of Energy and the National Science Foundation under Grant No. PHY-1430152 (JINA Center for the Evolution of the Elements).

References

[1] S. Amari, X. Gao, L.R. Nittler, E. Zinner, J. José, M. Hernanz, R.S. Lewis, Astrophys. J. 551 (2001) 1065.
[2] B.B. Back, J.A. Clark, R.C. Pardo, K.E. Rehm, G. Savard, AIP Adv. 4 (2014) 041005.
[3] D.W. Bardayan, K.A. Chipps, S. Ahn, J.C. Blackmon, R.J. deBoer, U. Greife, K.L. Jones, A. Kontos, R.L. Kozub, L. Linhardt, B. Manning, M. Matos, P.D. O'Malley, S. Ota, S.D. Pain, W.A. Peters, S.T. Pittman, A. Sachs, K.T. Schmitt, M.S. Smith, P. Thompson, Phys. Lett. B 751 (2015) 311.
[4] H. Becker, L. Buchmann, J. Gorres, K. Kettner, H. Krwinkel, C. Rolfs, P. Schmalbrock, H. Trautvetter, A. Vlieks, Nucl. Instr. Meth. 198 (1982) 277.
[5] M.B. Bennett, C. Wrede, K.A. Chipps, J. Jose, S.N. Liddick, M. Santia, A. Bowe, A.A. Chen, N. Cooper, D. Irvine, E. McNeice, F. Montes, F. Naqvi, R. Ortez, S.D. Pain, J. Pereira, C. Prokop, J. Quaglia, S.J. Quinn, S.B. Schwartz, S. Shanab, A. Simon, A. Spyrou, E. Thiagalingam, Phys. Rev. Lett. 111 (2013) 232503.
[6] G. Bittner, W. Kretschmer, W. Schuster, Nucl. Instr. Meth. 167 (1979) 1.
[7] E.M. Burbidge, G.R. Burbidge, W.A. Fowler, F. Hoyle, Rev. Mod. Phys. 29 (1957) 547.
[8] A.E. Champagne, C. Iliadis, R. Longland, AIP Adv. 4 (2014) 041006.
[9] K.A. Chipps, U. Greife, D.W. Bardayan, J.C. Blackmon, A. Kontos, L.E. Linhardt, M. Matos, S.D. Pain, S.T. Pittman, A. Sachs, H. Schatz, K.T. Schmitt, M.S. Smith, P. Thompson, the JENSA Collaboration, Nucl. Instr. Meth. A 763 (2014) 553.
[10] K.A. Chipps, S.D. Pain, U. Greife, R.L. Kozub, D.W. Bardayan, J.C. Blackmon, A. Kontos, L.E. Linhardt, M. Matos, S.T. Pittman, A. Sachs, H. Schatz, K.T. Schmitt, M.S. Smith, P. Thompson, Phys. Rev. C 92 (2015) 034325.
[11] K.A. Chipps (PI), experiment E15232 proposed to NSCL/ReA3 PAC39, May 2015.
[12] E. Churazov, R. Sunyaev, J. Isern, J. Knodlseder, P. Jean, F. Lebrun, N. Chugai, S. Grebenev, E. Bravo, S. Sazonov, M. Renaud, Nature 512 (2014) 406.
[13] J.J. Cowan, C. Sneden, Nature 440 (2006) 1151.
[14] A.M. Davis, Proc. Nat. Acad. Sci. U.S.A. 108 (2011) 19142.
[15] B. Davids, AIP Adv. 4 (2014) 041003.
[16] R. Diehl, J. Knodlseder, K. Bennett, H. Bloemen, C. Dupraz, W. Hermsen, G.G. Lichti, D. Morris, U. Oberlack, J. Ryan, V. Schonfelder, H. Steinle, A.W. Strong, M. Varendoff, C. Winkler, Adv. Space. Res. 15 (1995) 123.
[17] R. Diehl, M. Cervino, D.H. Hartmann, K. Kretschmer, New Astron. Rev. 48 (2004) 81.
[18] R. Diehl, H. Halloin, K. Kretschmer, G.G. Lichti, V. Schonfelder, A.W. Strong, A. von Kienlin, W. Wang, P. Jean, J. Knodlseder, J.-P. Roques, G. Weidenspointner, S. Schanne, D.H. Hartmann, C. Winkler, C. Wunderer, Nature (London) 439 (2006) 45.
[19] T. Griegel, H.W. Drotleff, J.W. Hammer, H. Knee, K. Petkau, J. Appl. Phys. 69 (1991) 19.
[20] F. Hammache, EJC2016, available at https://ejc2016.sciencesconf.org/conference/ejc2016/pages/Hammache_abstract_EJC2016.pdf.
[21] C. Iliadis, A. Champagne, A. Chieffi, M. Limongi, Ap. J. Suppl. Series 193 (2011) 16.
[22] J. Jose, M. Hernanz, S. Amari, K. Lodders, E. Zimmer, Astrophys. J. 612 (2004) 414.
[23] A.M. Laird, Nuclei in the Cosmos XII, PoS(NIC XII)014 (2012).

[24] Z. Meisel, K. Shi, A. Jemcov, M. Couder, Nucl. Instr. Meth. A 828 (2016) 8.
[25] MINBAR online x-ray burst light curve library, available at http://burst.sci.monash.edu/minbar/, accessed January 2017.
[26] S.D. Pain, AIP Adv. 4 (2014) 041015.
[27] S.D. Pain, D.W. Bardayan, J.C. Blackmon, S.M. Brown, K.Y. Chae, K.A. Chipps, J.A. Cizewski, K.L. Jones, R.L. Kozub, J.F. Liang, C. Matei, M. Matos, B.H. Moazen, C.D. Nesaraja, J. Okolowicz, P.D. O'Malley, W.A. Peters, S.T. Pittman, M. Ploszajczak, K.T. Schmitt, J.F. Shriner Jr., D. Shapira, M.S. Smith, D.W. Stracener, G.L. Wilson, Phys. Rev. Lett. 114 (2015) 212501.
[28] K. Schmid, L. Veisz, Rev. Sci. Instrum. 83 (2012) 053304.
[29] SRIM/TRIM semi-empirical stopping power code, available at www.srim.org, accessed January 2017.
[30] W. Tietsch, K. Bethge, H. Feist, E. Schopper, Nucl. Instr. Meth. 158 (1979) 41.
[31] R.E. Tribble, C.A. Bertulani, M. La Cognata, A.M. Mukhamedzhanov, C. Spitaleri, Rep. Prog. in Phys. 77 (2014) 106901.
[32] VIKAR monte-carlo nuclear reaction simulation code, written by S.D. Pain, available at https://sites.google.com/a/nuclearemail.org/vikar/, accessed January 2017.
[33] C. Wrede, AIP Adv. 4 (2014) 041004.
[34] E. Zinner, Annu. Rev. Earth Planet. Sci. 26 (1998) 147.